

Magnetic exchange interactions and critical temperature of the nanolaminate Mn_2GaC from first-principles supercell methods

A. Thore,^{1,*} M. Dahlqvist,^{1,†} B. Alling,^{1,2,‡} and J. Rosen^{1,§}¹*Department of Physics, Chemistry and Biology, Thin Film Physics Division, Linköping University, SE-581 83 Linköping, Sweden*²*Department of Computational Materials Design, Max-Planck-Institut für Eisenforschung GmbH,**Max-Planck-Straße 1, 40237 Düsseldorf Nordrhein-Westfalen, Germany*

(Received 27 August 2015; revised manuscript received 21 December 2015; published 29 February 2016)

In this work, we employ and critically evaluate a first-principles approach based on supercell calculations for predicting the magnetic critical order-disorder temperature T_c . As a model material we use the recently discovered nanolaminate Mn_2GaC . First, we derive the exchange interaction parameters J_{ij} between pairs of Mn atoms on sites i and j of the bilinear Heisenberg Hamiltonian using the novel magnetic direct cluster averaging method (MDCA), and then compare the J 's from the MDCA calculations to the same parameters calculated using the Connolly-Williams method. We show that the two methods yield closely matching results, but observe that the MDCA method is computationally less effective when applied to highly ordered phases such as Mn_2GaC . Secondly, Monte Carlo simulations are used to derive the magnetic energy, specific heat, and T_c . For Mn_2GaC , we find $T_c = 660$ K. The uncertainty in the calculated T_c caused by possible uncertainties in the J 's is discussed and exemplified in our case by an analysis of the impact of the statistical uncertainties of the MDCA-derived J 's, resulting in a T_c distribution with a standard deviation of 133 K.

DOI: [10.1103/PhysRevB.93.054432](https://doi.org/10.1103/PhysRevB.93.054432)

I. INTRODUCTION

The magnetic critical order-disorder temperature T_c , which encompasses both the Curie temperature T_C for ferromagnetic (FM) materials and the Néel temperature T_N for antiferromagnetic (AFM) materials, is of fundamental importance for the functionality of magnetic devices under realistic working conditions. An active area of research in materials science is the development of first-principles based methods which qualitatively and quantitatively describe the interactions that govern the magnetic properties of a material, including T_c [1]. One important aim of this research is to enable accurate and time-efficient computational screening for materials with magnetic transition temperatures suitable for technological applications. The quantum-mechanical nature of the problem makes this endeavor a challenging task, and so far experimental trends in T_c with, e.g., chemical composition, have generally been easier to accurately reproduce and predict than specific values of T_c , although examples of quantitatively accurate results for different materials systems are occasionally reported [2–6].

Adding to the challenge is the question of whether the investigated materials should be treated according to the itinerant or localized model of magnetism, or whether it is necessary to invoke the more general theory of spin density fluctuations introduced by Moriya, in which the itinerant and localized magnetic moment models are limiting cases [7]. However, for many magnetic solids where $3d$ transition metals are responsible for the magnetic properties, the d -band electrons, while itinerant, are still fairly strongly bounded to their respective sites [1,8]. Thus, for these materials, the

localized model, where the electronic spins close to the atomic nuclei are viewed collectively as a single, localized magnetic moment that interacts with the moments of the other sites in the lattice, is a good approximation [9]. This is convenient for calculations of T_c , as it allows for the magnetic energy of any magnetic configuration to be mapped onto a Heisenberg Hamiltonian. In its simplest form, this Hamiltonian takes into account only bilinear interaction terms, and can be expressed as

$$H = - \sum_{i \neq j} J_{ij} \mathbf{e}_i \cdot \mathbf{e}_j, \quad (1)$$

where the parameter J_{ij} is the magnitude of the magnetic exchange interaction (MEI) between atoms i and j , and \mathbf{e}_i and \mathbf{e}_j are unit vectors parallel to the respective magnetic moments of these atoms. The Heisenberg Hamiltonian can be evaluated at a range of different temperatures by randomly changing the relative directions of \mathbf{e}_i and \mathbf{e}_j using, for instance, Monte Carlo simulations. The magnetic critical temperature T_c can then be found directly from the peak of the heat capacity or magnetic susceptibility curve.

The MEI parameters J_{ij} can be calculated through, e.g., methods based on the magnetic force theorem [10–13], or supercell methods such as the frozen magnon method [14], the Connolly-Williams method (CW) [15,16], or the ones used by Fedorova *et al.* in Ref. [17]. In this work, however, we critically evaluate a novel supercell method for calculating MEI parameters, the magnetic direct cluster averaging method (MDCA), which was recently developed by Lindmaa *et al.* to handle chemically and topologically disordered phases [18]. We apply both the MDCA method and, for comparison, the CW method, to a structurally completely ordered phase, the magnetic MAX phase Mn_2GaC , whose existence was predicted from first-principles calculations and subsequently verified experimentally by Ingason *et al.* [19]. For this phase, use of the localized model of magnetism, and hence a Heisenberg Hamiltonian to represent the magnetic energy,

*Corresponding author: andth@ifm.liu.se

†madah@ifm.liu.se

‡bjoal@ifm.liu.se

§johro@ifm.liu.se

is justified by its strong local Mn moments, as discussed in Sec. III A.

Mn₂GaC belongs to the so-called MAX family (M = early transition metal, A = A-group element, and X = C and/or N), which to date consists of more than 70 nanolaminated, hexagonal phases. It is one of the first MAX phases to exhibit magnetism [19,20], and together with its potential for magnetocaloric applications, an in-depth exploration of the magnetism of this phase is highly interesting. Previous theoretical and experimental work on Mn₂GaC has focused on the influence on its magnetic behavior of both applied magnetic fields and temperature, and it has been shown that the phase is magnetic up to at least 300 K [19,21]. In the present study we use the MDCA-derived MEI parameters in Monte Carlo simulations to predict an order-disorder temperature of 660 K. We also discuss how accurate first-principles based calculations of T_c can be expected to be, given uncertainties in the values of the MEI parameters. Here we exemplify this by considering $T_c = 660$ K as the mean of a Gaussian distribution caused by the MDCA-specific statistical uncertainties in the J 's, and calculating a standard deviation of 133 K for this distribution.

II. CALCULATION DETAILS

The basic concept of the MDCA method is virtually identical to that of the direct cluster averaging (DCA) method for calculating chemical effective pair interactions in binary alloys first proposed by Berera *et al.* [22,23], the only difference being that the site variable in MDCA is the atomic magnetic moment instead of the atomic species. As described in Ref. [18], to find J_{ij} for two atoms i and j , we generate a large number of supercells σ_k ($k = 1, \dots, n$) in which the magnetic moments of the other $N - 2$ atoms have been assigned spatial directions through a randomization procedure. For each σ_k , an electronic structure relaxation is performed to obtain the total energy for a set of different, but fixed, directions of atoms i and j . This set is the same for all σ_k . The approximation in Eq. (1), which only includes bilinear interactions, entails that we can restrict ourselves to collinear magnetic configurations. This means that there are only four possible ways to fix the relative directions of the magnetic moments of atoms i and j : $\uparrow\uparrow$, $\downarrow\downarrow$, $\uparrow\downarrow$, and $\downarrow\uparrow$. Thus the MEI between atoms i and j for a single, randomly generated supercell σ_k is given by

$$J_{ij}^{\sigma_k} = -\frac{1}{8}(E_{\uparrow\uparrow} + E_{\downarrow\downarrow} - E_{\uparrow\downarrow} - E_{\downarrow\uparrow}), \quad (2)$$

since all interactions between the moments of atoms i and j with any other atom in σ_k are canceled out by the averaging over the four spin-pair directions. However, the final value of J_{ij} is not obtained until all possible multisite interactions have also been canceled out. This is ideally done by averaging over the entire magnetic configuration space, but in practice, due to its immense size (2^{N-2} possible configurations for each atomic pair), statistical sampling is necessary. We thus get

$$J_{ij} \approx \frac{1}{n} \sum_{k=1}^n J_{ij}^{\sigma_k}, \quad (3)$$

where n is the size of a subset of the magnetic configuration space. The sampling entails that each pair interaction will be

associated with a sampling error, here assumed to follow a t distribution. The corresponding confidence intervals can be expressed as

$$\Delta J_{ij} = \pm t_{\alpha/2}(f) \frac{s}{\sqrt{n}}, \quad (4)$$

where $t_{\alpha/2}(f)$ is a two-tailed t distribution of significance level α with $f = n - 1$ degrees of freedom, s is the sample standard deviation, and the fraction s/\sqrt{n} is the sampling distribution standard deviation.

For each supercell σ_k , the four energy terms in Eq. (2) were determined through electronic energy minimization with the ions fixed in the calculated 0 K geometry of AFM[0001]₂^A Mn₂GaC, which exhibits a layered AFM configuration with two consecutive Mn layers with parallel spins along the [0001] direction that change sign upon crossing a Ga layer (hence “A2”), as shown in Fig. 1(a) [20]. The formation enthalpy for this configuration (−30 meV/atom) is just below that for FM Mn₂GaC (−29 meV/atom), and just above that for a second AFM spin configuration denoted AFM[0001]₄^A (−31 meV/atom), which differs from AFM[0001]₂^A in that it has four consecutive Mn layers with parallel spins, instead of two, before flipping spins upon passing a Ga layer [20]. While these three spin configurations, which all have slightly different lattice geometries, are nearly degenerate in energy, we chose the geometry associated with the AFM[0001]₂^A configuration for three reasons: (i) magnetization measurements so far seem to preclude a purely FM configuration, but rather point to the phase being AFM; (ii) the match between a simulated x-ray diffraction spectrum and the experimental room temperature spectrum is closer for AFM[0001]₂^A Mn₂GaC than for both FM and AFM[0001]₄^A; and (iii) the lattice parameters for AFM[0001]₂^A Mn₂GaC more closely match the experimental ones measured at room temperature [20,21].

In the AFM[0001]₂^A geometry all Mn sites are equivalent, and it is therefore sufficient to calculate only one J per coordination shell. The arrows in Figs. 1(b) and 1(c) point to Mn atoms in the 11 first coordination shells, where the 11th shell corresponds to a length of ~ 7.13 Å. In this case, interactions involving Mn atoms in the eighth, ninth, and tenth coordination shells also include a mirror image contribution that doubles the obtained interaction strength, thus requiring the resulting J to be divided by a factor of 2. Ideally, supercells large enough to avoid significant mirror image interactions should be used, but since we use $4 \times 4 \times 1$ supercells with 128 atoms in total, increasing the size further would have resulted in impractically high computational times.

In the CW method, the MEI parameters are instead obtained by solving a system of equations consisting of the Heisenberg Hamiltonians for several different magnetic configurations. In this case, the Heisenberg Hamiltonian given by Eq. (1) is rewritten as

$$H = - \sum_{\alpha} J_{\alpha} n_{\alpha} \Phi_{\alpha}, \quad (5)$$

where n_{α} is the number of magnetic atoms in the α th coordination shell and Φ_{α} the corresponding correlation function. For a set of different magnetic configurations, one can obtain J_{α} by calculating the electronic energy for each magnetic configuration as well as their respective sets of correlation

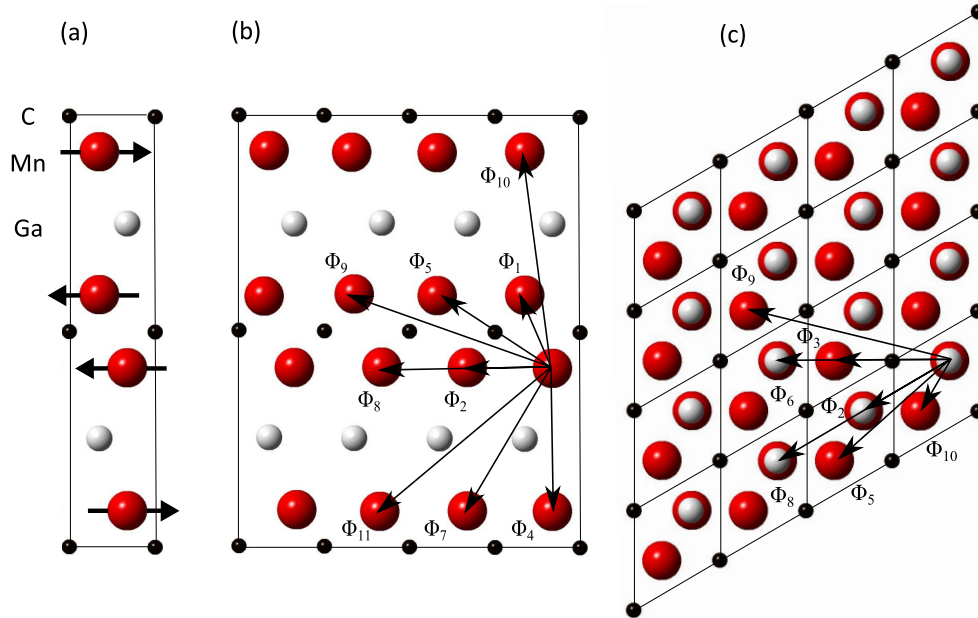


FIG. 1. (a) Schematic representation of the AFM $[0001]_2^4$ magnetic configuration. (b), (c) Side and top view, respectively, of a $4 \times 4 \times 1$ Mn_2GaC supercell, with arrows pointing to atoms in each of the 11 different coordination shells Φ_α considered in this work.

functions and n_α (which, for a given shell α , is the same for all configurations), and then perform a least-squares fit on the equation system [15]. The CW method is particularly well suited for chemically ordered MAX phases, since the α th coordination shell with respect to each magnetic M atom then always contains neighboring magnetic M atoms at the same relative locations, i.e., n_α is independent of the M atom for which Φ_α is to be determined.

All electronic energy minimizations in this work have been carried out within the framework of density functional theory [24] as implemented in the Vienna *ab initio* simulation package (VASP) [25–28], using the Perdew-Burke-Ernzerhof exchange-correlation energy functional [29], and the projector augmented wave method for solving the Kohn-Sham equations [14,15]. The Brillouin zones of all of the $4 \times 4 \times 1$, 128-atom supercells were sampled using a Γ -centered $3 \times 3 \times 3$ Monkhorst-Pack k -point grid, and the cutoff energy was set to 400 eV.

The magnetic energy given by Eq. (1) was minimized by running Metropolis-type semiclassical Heisenberg Monte Carlo simulations [30] using the MDCA-derived MEI parameters and 32 000 Mn atoms, for temperatures in the interval of 20–1000 K. At each temperature step, 30 000 random spin flips were performed, out of which the trailing 24 000 were collected (to avoid remnant effects from the previous step).

III. RESULTS AND DISCUSSION

A. Mn magnetic moments

Figure 2 shows a histogram of the local Mn magnetic moments for all randomly generated magnetic configurations, after the electronic structure relaxations, after the electronic structure relaxations. The vast majority of these moments have magnitudes of at least $1.5\mu_B$, and for all but a tiny fraction of them, the spatial orientation is the same as the orientation before the relaxations. The variation in the

strengths of the local moments is not due to the longitudinal spin fluctuations characteristic of itinerant magnets, but is here instead caused by variations in the local magnetic environment. Strong local moments are consistent with the localized model of magnetism (where only transverse spin fluctuations are important), but not with the itinerant model.

B. Magnetic exchange interaction parameters

Three different sets of MEI parameters for a number of coordination shells α are shown in Fig. 3. One set has been calculated using the MDCA method, while for the other two sets the CW method has been used. The CW parameters were determined from two different sets of magnetic spin

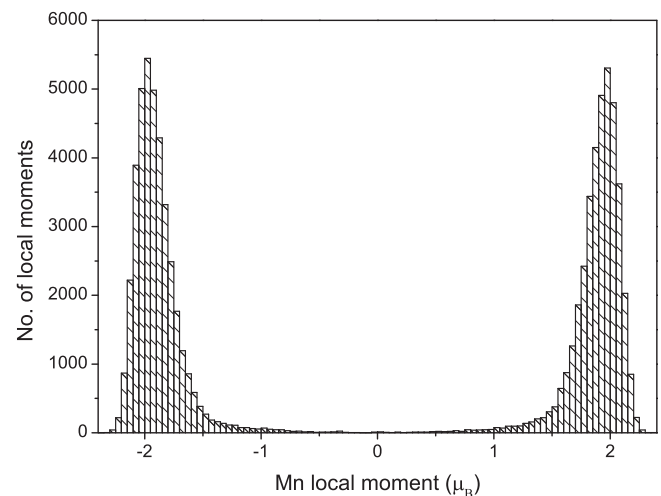


FIG. 2. The local Mn moments for different, randomly generated magnetic configurations, after electronic structure relaxations have been performed.

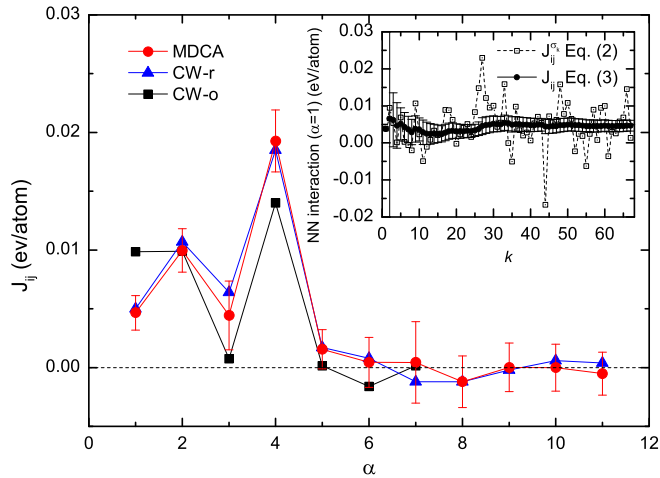


FIG. 3. Magnetic exchange interaction parameters derived using the MDCA method and the Connolly-Williams method, the latter applied both to a large set of randomly generated magnetic configurations (CW-r) and a smaller set of ordered configurations (CW-o). The inset shows the nearest neighbor ($\alpha = 1$) MEI parameters for each of the randomly generated magnetic supercell configurations (open squares), together with the cumulative moving average (closed circles) and its associated 95% confidence intervals.

configurations: the ones also used in the calculations of the MDCA parameters, for which the correlation functions Φ_α generally are very small due to the low probability of generating magnetically ordered shells using a randomizing procedure, and manually constructed ordered ones (FM as well as different AFM spin configurations); these sets are denoted CW-r and CW-o, respectively. For the CW-o parameters only the first seven coordination shells have been considered as the relatively low number of included configurations significantly limited the accuracy of the MEI parameters for the more long-ranged shells.

By comparing the MDCA with the CW-o MEI parameters, we see that, while the trends are similar, some of the short-range interactions differ significantly between the two parameter sets, e.g., J_1 differs by a factor of 2. If we instead compare the MDCA MEI parameters to the CW-r ones, we see that the differences are small, with each CW-r parameter lying within the 95% confidence interval calculated for the corresponding MDCA parameter.

This discrepancy exemplifies a potential pitfall when calculating MEI parameters: the obtained J 's are strongly dependent on the magnetic reference state, i.e., whether it is ordered or disordered. This may in turn have an impact on the accuracy of the magnetic thermodynamics calculated from the J 's. For MEI parameters derived from a set of ordered spin configurations, a calculation of the energy of a highly disordered state is likely to be less accurate than if the input set instead consists predominantly of low-order spin configurations, and vice versa [31]. Hence, since we are interested in the energy around the order-disorder temperature, the set of CW-r parameters should be the preferred choice as a reference set with respect to the MDCA parameters. The good agreement between the MDCA and CW-r parameter sets

suggests that either method may be used. However, in addition to accuracy, the computational cost is an important factor.

As illustrated by the inset in Fig. 3, the size of each confidence interval of the MDCA parameters depends on the number of terms $J_{ij}^{\sigma k}$ included in Eq. (3). Using current state-of-the-art hardware, calculating even one such term is quite costly, and we have therefore restricted our calculations to $k \sim 20$ for all coordination shells except for the first one ($\alpha = 1$), for which $k = 67$ as a test case (80 supercells were generated initially, but 13 were discarded due to spin flips during the calculations). For ordered phases like Mn_2GaC this is a practical limitation of the MDCA method, which makes it less suitable than the CW method for determining MEI parameters. Using the CW method, reliable parameter values up to the 11th coordination shell could be obtained for as few as ~ 20 of the randomly generated supercells. This shows the importance of carefully choosing which method to apply. As discussed by Lindmaa *et al.* in Ref. [18], the MDCA method gives direct access to any specific pair interaction, thus making it highly suitable for phases in which several or all magnetic atoms occupy unique lattice sites, such as chemically disordered or amorphous phases.

C. Critical temperature of Mn_2GaC

The curves in Fig. 4(a) show the specific heat C_v for Mn_2GaC in the interval of 0–1000 K, obtained from Monte Carlo simulations of Eq. (1) using the MDCA-derived MEI parameters seen in Fig. 4. It is clear from the figure that the location of the peak of C_v , and hence the critical temperature

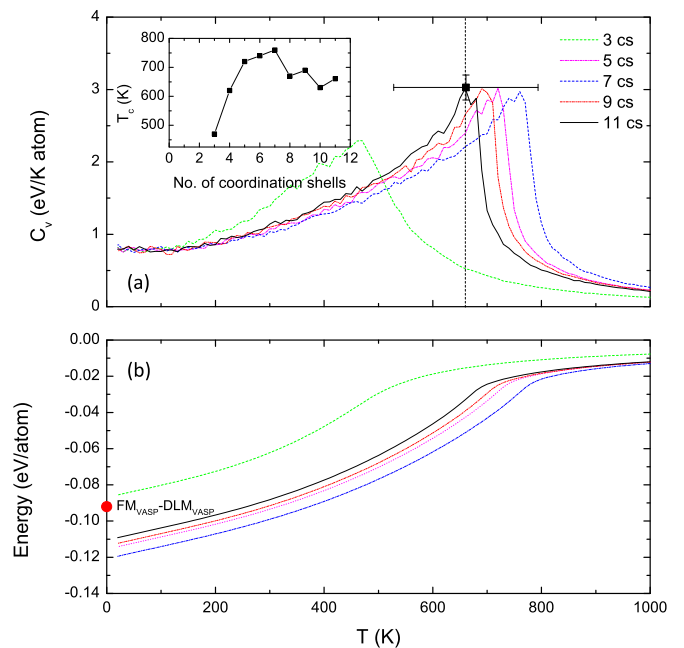


FIG. 4. (a) Specific heat as a function of temperature for the MDCA MEI parameters for increasing numbers of coordination shells (cs). The horizontal and vertical error bars belonging to the 11 cs peak are the standard deviations for T_c and C_v , respectively. Inset: convergence of T_c as a function of the number of considered coordination shells. (b) The magnetic energy. The difference between FM and PM (DLM) VASP energies is indicated by the closed circle.

T_c (which coincides with this peak), is very sensitive to the number of coordination shells considered. For instance, if the MEI parameters for only the first three coordination shells are included, T_c is found at 450 K, whereas for 11 coordination shells it is found at 660 K. This further shows that, even as the strengths of the individual interactions begin to vanish—which in this case happens beyond the fourth coordination shell, as seen in Fig. 3—they may collectively contribute to a non-negligible effect on T_c . Also, the possibility exists that long-range interactions that have not been considered may actually be strong enough to have a significant impact. However, an argument that $T_c = 660$ K should be reasonably close to the real value can be made from an analysis of the temperature-dependent free energy curves, which are shown in Fig. 4(b). The difference in energy between 20 K, which corresponds to a FM spin configuration, and infinity, where the magnetic energy is 0 eV and thus corresponds to a perfect paramagnetic (PM) spin configuration, varies from -0.085 to -0.12 eV/atom depending on the number of coordination shells considered. This is close to the result from our 0 K VASP calculations, which, when the AFM[0001]₂^A geometry is used, yield an energy difference of -0.092 eV/atom between FM and PM Mn₂GaC [the PM spin configuration was modeled by a disordered local moment (DLM) state [32,33]]. We note here that an exact agreement with the VASP result should not be expected due to the fact that the MDCA MEI parameters were derived from highly disordered states, and therefore likely do not describe the low-temperature magnetic behavior of the phase entirely accurately, as discussed in the previous section.

Given a set of MEI parameters, converging MEI parameter-dependent properties such as T_c is thus merely a matter of considering enough coordination shells. However, the accuracy of the converged properties depend on the accuracy of the MEI parameters, the latter which can be affected by several possible factors. Examples of such factors are lattice vibrations, thermal expansion, electronic excitations, and structural defects like vacancies and impurities. Factors related to the tools and methods used may also influence the accuracy, such as various approximations implemented in density functional theory (the exchange-correlation functionals in particular) as well as the choice of Hamiltonian onto which the magnetic energy is mapped. For a few materials systems, efforts have been undertaken to estimate the impact of some of these factors on the MEI parameters and the degree to which this propagates to the properties derived from the parameters [11,14,17,32]. For instance, in Ref. [11] Alling *et al.* have investigated the dependence of the Curie temperature of the half-Heusler Ni_{1-x}Cu_xMnSb alloy on, e.g., thermal expansion, structural defects, and choice of magnetic reference state used in the derivation of the MEI parameters. They found that by going from room temperature to ~ 1000 K, the lattice parameter increases by $\sim 1\%$, which—depending on whether the magnetic reference state is DLM or FM—in turn can lead to as much as a 15% decrease in the Curie temperature. While this is certainly significant, it is unclear whether these results are directly transferable to Mn₂GaC, one reason being that the coefficient of thermal expansion for this phase may be different. However, although it would certainly be worthwhile to study the impact on T_c for Mn₂GaC of thermal expansion as well as of other internal and external factors, we have in this

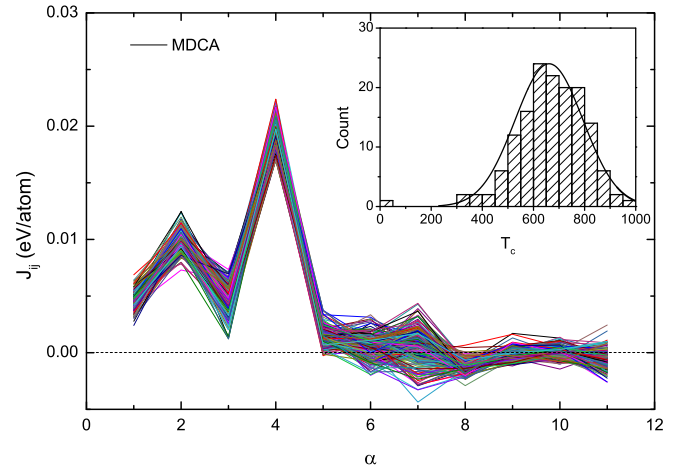


FIG. 5. Sets of MEI parameters generated using the MDCA parameters in Fig. 3 as mean values of a Gaussian distribution, each with a standard deviation given by s/\sqrt{n} in Eq. (4). Inset: the resulting histogram of T_c 's, with a Gaussian fit superimposed.

work limited our focus to an investigation of a method-related factor specific to the MDCA method: the effect on T_c of the errors in the J 's that arise due to the sampling of magnetic configuration space.

This is illustrated in Fig. 5 for 150 different sets of MEI parameters, where each parameter value for a given coordination shell α has been generated from a Gaussian distribution centered on the corresponding MDCA-derived J (see Fig. 3) which is here taken to be a good estimate of the sample mean for that specific J . The standard deviation for each J is given by the sampling distribution standard deviation s/\sqrt{n} in Eq. (4). Carrying out a Monte Carlo simulation for each set results in the histogram of different T_c 's shown in the inset of Fig. 5, with $T_c = 660$ K as the mean temperature. By fitting the histogram with a Gaussian distribution the standard deviation is 133 K (20%) in each direction, shown as an error bar in Fig. 4(a). The uncertainty in T_c is thus quite significant, despite the relatively small differences between the MEI parameter sets. We want to emphasize that even though the uncertainties in the J 's obtained here stem from a particular methodological aspect of the MDCA method, uncertainties in first-principles calculated J 's are always present to at least some degree due to the factors discussed in the previous paragraph. Thus, our finding, i.e., that an uncertainty of a few meV in the magnitudes of the MEI parameters transforms into an uncertainty of hundreds of K in T_c , should be of importance for every future study attempting to predict order-disorder critical temperatures from first principles, irrespective of material.

Nevertheless, for Mn₂GaC, $T_c = 660 \pm 133$ K, which is not in conflict with present experimental results. Vibrating sample magnetometry measurements have shown the phase to exhibit a magnetic response at least up to room temperature [21]. We also note that similar experimental results have been reported for quaternary MAX phases with a solid solution of Cr and Mn on the M sublattice. For example, Mockuté *et al.* found (Cr_{1-x}Mn_x)₂GaC with $x = 0.3$ to give a magnetic response up to the maximum measurement temperature of 300 K, as did

both Petruhins *et al.* for $(\text{Cr}_{1-x}\text{Mn}_x)_2\text{GaC}$ with $x = 0.5$ and Ingason *et al.* for $(\text{Cr}_{1-x}\text{Mn}_x)_2\text{GeC}$ with $x = 0.25$ [34–36]. We additionally note that further work on $(\text{Cr}_{1-x}\text{Mn}_x)_2\text{GeC}$ by Tao *et al.* has shown that T_c of this phase increases with increasing Mn content [37].

IV. CONCLUSIONS

In conclusion, we have used the novel magnetic direct cluster averaging method to calculate magnetic exchange interaction parameters for 11 different coordination shells in the magnetic MAX phase Mn_2GaC . The MEI parameters were then used as input in Monte Carlo simulations to predict the critical magnetic order-disorder temperature.

The MEI parameters were shown to be in good agreement with a reference parameter set calculated using the Connolly-Williams method. However, for ordered phases like Mn_2GaC , the MDCA method is associated with a significantly higher computational cost than the CW method.

The critical temperature was predicted to be 660 K, with a standard deviation of 133 K stemming from the statistical

nature of the MDCA method. Still, experimental measurements on both Mn_2GaC as well as on related MAX phases are presently not in conflict with the theoretical results presented here.

ACKNOWLEDGMENTS

Professor Andrei Ruban is acknowledged for useful discussions on the Monte Carlo code. This research was funded by the European Research Council under the European Community Seventh Framework Program (FP7/2007-2013)/ERC Grant agreement No. 258509. J.R. acknowledges funding from the Swedish Research Council (VR), from the Knut and Alice Wallenberg (KAW) Fellowship program, and from the SSF synergy grant FUNCASE. B.A. acknowledges funding from the Swedish Research Council (VR) Grant No. 621-2011-4417 and 330-2014-6336. The calculations were carried out using supercomputer resources provided by the Swedish National Infrastructure for Computing (SNIC) at the National Supercomputer Centre (NSC), and the High Performance Computer Center North (HPC2N).

-
- [1] I. A. Abrikosov, A. V. Ponomareva, P. Steneteg, S. A. Baranikova, and B. Alling, *Current Opinion in Solid State and Materials Science* (in press), Corrected Proof, Available online 13 August 2015.
 - [2] B. Alling, *Phys. Rev. B* **82**, 054408 (2010).
 - [3] T. Fukushima, K. Sato, H. Katayama-Yoshida, and P. H. Dederichs, *Jpn. J. Appl. Phys.* **43**, L1416 (2004).
 - [4] V. V. Sokolovskiy, V. D. Buchelnikov, M. A. Zagrebin, P. Entel, S. Sahoo, and M. Ogura, *Phys. Rev. B* **86**, 134418 (2012).
 - [5] O. Schilling, *Braz. J. Phys.* **43**, 214 (2013).
 - [6] T. Graf, S. S. P. Parkin, and C. Felser, *IEEE Trans. Magn.* **47**, 367 (2011).
 - [7] T. Moriya, *J. Magn. Magn. Mater.* **14**, 1 (1979).
 - [8] J. Kübler, *Theory of Itinerant Electron Magnetism* (Oxford University Press, Oxford, 2000).
 - [9] E. Sjöstedt and L. Nordström, *Phys. Rev. B* **66**, 014447 (2002).
 - [10] A. I. Liechtenstein, M. I. Katsnelson, and V. A. Gubanov, *J. Phys. F: Met. Phys.* **14**, L125 (1984).
 - [11] B. Alling, A. V. Ruban, and I. A. Abrikosov, *Phys. Rev. B* **79**, 134417 (2009).
 - [12] A. V. Ruban, S. Shallcross, S. I. Simak, and H. L. Skriver, *Phys. Rev. B* **70**, 125115 (2004).
 - [13] S. Keshavarz, Y. O. Kvashnin, I. Di Marco, A. Delin, M. I. Katsnelson, A. I. Liechtenstein, and O. Eriksson, *Phys. Rev. B* **92**, 165129 (2015).
 - [14] L. M. Sandratskii, R. Singer, and E. Şaşıoğlu, *Phys. Rev. B* **76**, 184406 (2007).
 - [15] J. W. D. Connolly and A. R. Williams, *Phys. Rev. B* **27**, 5169 (1983).
 - [16] R. Drautz and M. Fähnle, *Phys. Rev. B* **69**, 104404 (2004).
 - [17] N. S. Fedorova, C. Ederer, N. A. Spaldin, and A. Scaramucci, *Phys. Rev. B* **91**, 165122 (2015).
 - [18] A. Lindmaa, R. Lizárraga, E. Holmström, I. A. Abrikosov, and B. Alling, *Phys. Rev. B* **88**, 054414 (2013).
 - [19] A. S. Ingason, A. Petruhins, M. Dahlqvist, F. Magnus, A. Mockute, B. Alling, L. Hultman, I. A. Abrikosov, P. O. Å. Persson, and J. Rosen, *Mater. Res. Lett.* **2**, 89 (2014).
 - [20] A. Thore, M. Dahlqvist, B. Alling, and J. Rosén, *J. Appl. Phys.* **116** 103511 (2014).
 - [21] M. Dahlqvist, A. S. Ingason, B. Alling, F. Magnus, A. Thore, A. Petruhins, A. Mockute, U. B. Arnalds, M. Sahlberg, B. Hjorvarsson, I. A. Abrikosov, and J. Rosen, *Phys. Rev. B* **93**, 014410 (2016).
 - [22] A. Berera, H. Dreysse, L. T. Willes, and D. de Fontaine, *J. Phys. F: Met. Phys.* **18**, L49 (1988).
 - [23] H. Dreysse, A. Berera, L. T. Wille, and D. de Fontaine, *Phys. Rev. B* **39**, 2442 (1989).
 - [24] P. Hohenberg and W. Kohn, *Phys. Rev.* **136**, B864 (1964).
 - [25] G. Kresse and J. Hafner, *Phys. Rev. B* **47**, 558 (1993).
 - [26] G. Kresse and J. Hafner, *Phys. Rev. B* **49**, 14251 (1994).
 - [27] G. Kresse and J. Furthmüller, *Comput. Mater. Sci.* **6**, 15 (1996).
 - [28] G. Kresse and J. Furthmüller, *Phys. Rev. B* **54**, 11169 (1996).
 - [29] J. P. Perdew, K. Burke, and M. Ernzerhof, *Phys. Rev. Lett.* **77**, 3865 (1996).
 - [30] N. Metropolis, A. W. Rosenbluth, M. N. Rosenbluth, A. H. Teller, and E. Teller, *J. Chem. Phys.* **21**, 1087 (1953).
 - [31] A. Seko, Y. Koyama, and I. Tanaka, *Phys. Rev. B* **80**, 165122 (2009).
 - [32] B. Alling, T. Marten, and I. A. Abrikosov, *Phys. Rev. B* **82**, 184430 (2010).
 - [33] B. L. Gyorffy, A. J. Pindor, J. Staunton, G. M. Stocks, and H. Winter, *J. Phys. F: Met. Phys.* **15**, 1337 (1985).
 - [34] A. Mockute, J. Lu, E. J. Moon, M. Yan, B. Anasori, S. J. May, M. W. Barsoum, and J. Rosen, *Mater. Res. Lett.* **3** 16 (2014).
 - [35] A. Petruhins, A. Ingason, J. Lu, F. Magnus, S. Olafsson, and J. Rosen, *J. Mater. Sci.* **50**, 4495 (2015).

- [36] A. S. Ingason, A. Mockute, M. Dahlqvist, F. Magnus, S. Olafsson, U. B. Arnalds, B. Alling, I. A. Abrikosov, B. Hjorvarsson, P. O. Å. Persson, and J. Rosen, *Phys. Rev. Lett.* **110**, 195502 (2013).
- [37] Q. Z. Tao, C. F. Hu, S. Lin, H. B. Zhang, F. Z. Li, D. Qu, M. L. Wu, Y. P. Sun, Y. Sakka, and M. W. Barsoum, *Mater. Res. Lett.* **2**, 192 (2014).